Measurement of the induced refractive index in a photothermorefractive glass by a liquid-cell shearing interferometer

Oleg M. Efimov, Leonid B. Glebov, and Hervé P. Andre

A liquid-cell shearing interferometer was developed to measure refractive-index variations (Δn) in transparent materials. The cell was filled with a liquid having a matched refractive index. The achieved resolution was better than 1/1000 of a fringe shift and resulted in a Δn measurement sensitivity down to 10^{-7} for 1-mm-thick samples. A refractive-index increment in photothermorefractive glass of up to 5×10^{-6} was observed after UV exposure at 325 nm. A refractive-index decrement of up to 1×10^{-3} was observed after thermal development of the exposed sample. It was proved that photothermorefractive glass obeys the reciprocity law; i.e., Δn depends on the UV dosage but does not depend on the irradiance.

OCIS codes: 090.2900, 100.2650, 120.3180, 160.2750, 260.5210, 350.5340.

1. Introduction

Intensive progress in lasers, optical communications, and data storage has challenged scientists to achieve perfection in optical components. These challenges have resulted in an active development of a wide variety of unconventional optical elements, including volume diffractive elements on the basis of Bragg gratings (see Ref. 1). However, creating reliable photosensitive materials for volume hologram recording has in turn created a lot of problems,[1] and the lack of such materials restricts the extensive use of Bragg gratings in optical design. The only Bragg gratings that have wide application are fabricated in silica fibers doped with germanium.[2,3] However, the low sensitivity of this material restricts its application to fiber devices. One of the new photosensitive materials for volume hologram recording is a photothermorefractive (PTR) glass. This is an inorganic silicate glass codoped with silver, cerium, and fluorine (see a survey of its properties in Ref. 4). Recently, Bragg gratings (both transmitting and reflecting) in PTR glass with extremely high diffraction efficiency and very high stability were described in Refs. 5 and 6.

Although efficient diffractive elements have been demonstrated, to our knowledge, no comprehensive study of photoinduced refraction in PTR glass has been undertaken and no reliable experimental data concerning the mechanism of refraction-index increment have been recorded. One of the problems that constrains these studies is the experimental difficulty of obtaining an accurate measurement of the induced refractive index in photosensitive media. The most reliable method of induced refraction measurement is the interferometric one in which the Mach–Zehnder interferometer is used (see, e.g., Ref. 7). However, there are some problems that complicate these measurements. The first is the consequence of the basic principles of interferometry, which detects the difference of optical paths of beams and cannot distinguish variations in the surface shape of a tested object from variations of its bulk refractive index. This feature implies the necessity of achieving a high quality of surface finish, i.e., phase fluctuations in the optical beam caused by the surface imperfections should be much less than the expected phase fluctuations caused by variations of the refractive index in the volume of the tested object. This requirement results in a dramatic rise in the cost of testing samples and restrains wide applications of the method. The second problem is the necessity of using a great num-

O. M. Efimov is with Light Processing and Technologies, Orlando, Florida 32817. L. B. Glebov (leon@creol.ucf.edu) and H. P. Andre are with the Center for Research and Education in Optics and Lasers, University of Central Florida, P.O. Box 162700, Orlando, Florida 32816-2700.

Received 4 June 2001; revised manuscript received 3 October 2001.

0003-6935/02/101864-08$15.00/0

ber of samples for measurements of photosensitivity, which is equal to the number of the desired measuring points for different conditions of exposure and development.

Thus our goal in this study is to develop a method for the accurate measurement of optical homogeneity and photoinduced volume refractive-index variations in transparent media that possess high sensitivity to volume refractive-index variations, low sensitivity to surface imperfections of a tested object, and high productivity, and to apply this method for the measurement of the induced index of refraction in PTR glass.

Technical approach. Four main approaches were utilized in this work to achieve the desired goal. The first was to submerge the tested specimen in a cell filled with a liquid that had a refractive index matched to that of the specimen. In this case, the impact of the surface imperfections of the sample would be decreased by the ratio of the refractive-index difference between the specimen and air and the specimen and the matching liquid. A realistic refractive-index mismatch could range from 10^{-3} to 10^{-2}. This means that the impact of surface imperfections could be mitigated with this approach by approximately a factor of from 500 to 50 times, respectively. The second approach was to use the walls of the cell as mirrors of a shearing interferometer; this enables a phase-shift measurement with the lowest requirements for vibrational insensitivity. Use of a laser source with high coherence length allows elimination of the phase compensation[8] and use of the shearing interferometer for measurements in the case of high phase shifts between interfering beams. A modification of the shearing interferometer in the form of a cell with a liquid crystal within it for achieving a controllable phase shift was recently published in Ref. 9. However, to the best of our knowledge, there has been no publication concerning the use of a shearing interferometer that addressed the use of a cell with the tested specimen inside it.

The third approach was the use of a specific geometry for specimen illumination in the process of induced refractive-index formation. This geometry took the form of a homogeneous stripe aligned in the direction perpendicular to the orientation of fringes in the interferometer. This geometry allowed us to detect the phase shift not only for a single fringe but for all fringes in the interference pattern. This dramatically increased the accuracy of these measurements through data averaging over a number of the interference fringes. The fourth approach involved the spatial profiling of the optical beam used for photoinduced transformations in the tested specimen in the direction along the interference fringes. This means that the each point on the exposed sample in this direction corresponds to the definite value of the exposing dosage. Consequently, a calibrated lateral distribution of exciting beam irradiance enabled measurement of an induced refractive-index dependence on exposing energy within the single specimen.

We demonstrate that a combination of these approaches results in a sensitive method of optical homogeneity and induced refractive measurements. We have used this in the following study of an induced refractive index in PTR glass that is subsequently developed for volume hologram recording.

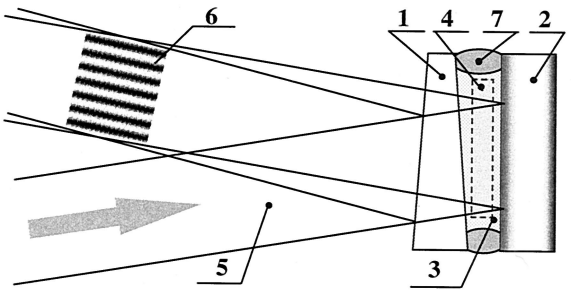

Fig. 1. Liquid cell for shearing interferometer: 1 and 2, front and back windows, respectively; 3, matching liquid; 4, sample; 5, laser probe beam; 6, interference pattern; 7, elastic gasket.

2. Experiment

A. Liquid Cell for Interferometric Measurements

The problem of distinguishing surface and volume phase distortions is important for interferometric measurements, especially when the quality of the sample surfaces machined under laboratory conditions results in a phase shift produced by the surface imperfections that is comparable with the phase shift produced by the volume refractive-index variations. The samples of PTR glass had a thickness $\sim$1 mm and flatness variations of $\sim$1 μm. In the case of the sample in an air environment, its thickness deviation of $\sim$1 μm that was due to poor surface finish would result in the same interference fringe shift in the interferometer as that of the internal refractive-index variation of $\sim 1.5 \times 10^{-3}$, which is comparable with the expected induced refraction.[4] Figure 1 shows the interferometric cell, which consists of two glass windows (1, 2) with high-quality surfaces (flatness $\sim\lambda/20$) filled with a liquid (3) having a refractive index matched to that of the tested specimen. The difference in the refractive indices between the tested specimen of PTR glass (4) and the matching liquid at the 633-nm wavelength was less than 3.5×10^{-3}. This decreased the phase shift caused by the distortions in the sample surfaces by a factor of $\sim$150 and resulted in an experimental error in the sixth decimal digit for measurement of the induced refractive index.

The beam of a He–Ne laser at 633 nm (5) reflected from the external surface of the front window (1) was used as a reference beam. The beam that was reflected from the front semitransparent surface of the back window (2) and passed two times through the sample (4) was used as an objective beam. It should be noted that the interaction of the low-intensity beams rereflected from the front and the rear windows of the cell resulted in a rather intense modulation of the main interference pattern, as was described in Ref. 8. To exclude the appearance of these parasitic fringes, the front window had the

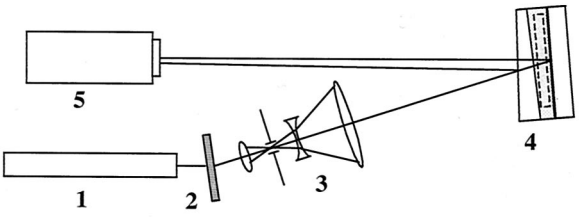

Fig. 2. Liquid-cell shearing interferometer: 1, He–Ne laser at 633 nm; 2, diffractive attenuator; 3, beam expander and spatial filter; 4, liquid cell; 5, CCD camera.

shape of a wedge while the back surface of the rear window was coated with an absorbing layer. Finally, the interference of the beams reflected from the front surfaces of both front and rear windows provided the interference pattern (6), which contained information about optical inhomogeneities in the bulk of the tested specimen. The interference pattern (6) consisted of the straight lines, and the pattern distortions were not detectable because high-quality windows were used to make the cell. Both windows (1, 2) of the cell were joined by an elastic gasket (7), and the cell mount provided an opportunity to adjust the front window with respect to the rear one. A gradual change in the angle between the reflecting surfaces allowed changing the spatial frequency of the fringes and allowed orienting them in a plane of observation.

B. Liquid-Cell Shearing Interferometric Setup

The interferometric setup for the refractive-index distribution measurements is shown in Fig. 2. The total power of the radiation from the He–Ne laser (1) at 633 nm was controlled by an attenuator (2) with variable transmission. Then the beam passed through a spatial filter–beam expander (3), reflected from the two surfaces of the liquid cell (4), and resulted in an interference pattern in the overlapping area of the beams. The interference pattern was recorded by a CCD camera (5). The attenuator (2) served to adjust the intensity of the interference pattern to be within the sensitivity range of the CCD camera (5). The total magnification of the spatial filter telescope was $\sim 60\times$, and this produced a uniformity of object illumination of better than 10% for the central part of the beam with a size of 10 mm $\times$ 10 mm. The two beams reflected from the liquid cell described in Subsection 2.A then recombined. One can see that this cell produces the effect of a lateral shearing interferometer. The interference pattern was detected with the CCD camera, stored in a computer, and processed with special software.

Precise positioning of the sample (± 10 μm) in the liquid cell (Fig. 1) was provided by the micrometer screws of the special sample holder mounted on the two-dimensional stage. This setup allowed us to repeat the measurement in the same area of the testing specimen and therefore determine repeatability of the measurement and compare the refractive-index profiles before and after irradiation.

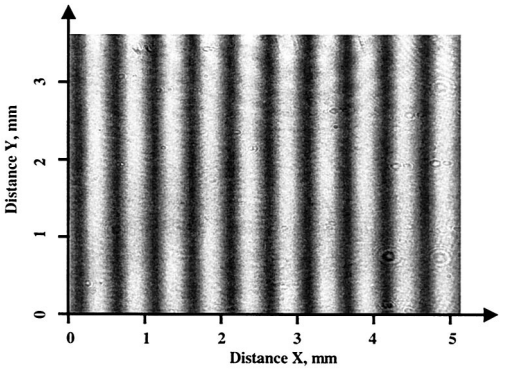

Fig. 3. Interference pattern from the virgin sample of PTR glass (1-mm thickness).

C. Exposure of the Sample to UV Radiation

Radiation from the cw He–Cd laser at 325 nm emitting a single transverse mode (Kimmon Electric, Model RM30211 R-L) was used for exposure of the samples. Both collimated and focused beams were used to provide different spatial distributions. The transverse distribution of intensity in the beam was determined by measurement of the intensity of the radiation transmitted through a pinhole of 50 μm in diameter, which was scanned across the beam. It was found that the transverse distribution of intensity could be fitted to a Gaussian function with an accuracy of better than 5%:

$$I(y) = I_{\max} \exp\left(-2\,\frac{y^2}{\omega^2}\right), \tag{1}$$

where y is the vertical coordinate (see Figs. 1, 3, and 5), $I(y)$ is the intensity distribution, $I_{\max}$ is the maximal intensity in the center of the beam at $y = 0$, and ω is the half-width of the beam at the level of $1/e^2$. This beam, having a Gaussian spatial profile, was directed onto a sample fixed on a motorized translational stage. While the sample was being exposed, the motorized stage scanned the sample with a constant speed V in the horizontal direction x (Fig. 3) perpendicular to the direction of the beam (z). Because of the motion of the stage, the irradiated area was a straight stripe in the x direction with a Gaussian distribution of dosage in the lateral y direction. It can be easily shown that the speed of translation V that provides the maximal dosage $D_{\max}$ on the center of the irradiated stripe is described by the following formula:

$$V = \sqrt{\frac{2}{\pi}}\,\frac{P}{\omega D_{\max}}, \tag{2}$$

where P is the total power of the laser beam. The dosage at any distance y from the center of the irradiated stripe will be described by

$$D(y) = D_{\max} \exp\left(-2\,\frac{y^2}{\omega^2}\right). \tag{3}$$

Thus each stripe recorded in the specimen possessed the same dosage along the x direction of the scanning laser beam and a continuous distribution of dosage in the perpendicular y direction, which was described by formula (3). This means that the averaging of the phase shift measured at the same distance from the center of the stripe (y is constant) allows accumulating data for the same dosage while measuring the phase shift versus distance from the center of the stripe (y is variable) provides the dependence of the induced index of refraction on the dosage. Typical values of speed of the scanning of 1-mW beam having ~2.5-mm width ranged from units to hundreds of micrometers per second to provide maximal dosage from hundredths to units of joules per square centimeter.

D. Sample Preparation

PTR glass was melted in accordance with the approach described in Ref. 5. Samples were cut from the glass slab, ground, and polished with a Buehler polishing station (Model Ecomet-3/Automet-2). The sample thickness was in the range of 1 mm, while the flatness of surfaces was approximately two wavelengths. Exposed samples underwent thermal development at 520 °C for a few hours to develop the induced refraction (see Ref. 4 for the process description). The surfaces were repolished after thermal development to eliminate imperfections caused by heat treatment.

3. Results and Discussion

A. Mapping of the Index of Refraction

An example of the interference pattern detected in the 1-mm sample of the virgin PTR glass is shown in Fig. 3. The interference fringes are oriented in the vertical direction (y). One can see a uniform interference pattern with a rather low level of noise. Any spatial fluctuations of the refractive index should cause interference fringe bending. The value and the direction of the fringe shift allows us to calculate the corresponding change of the refractive index in the tested area.

The formula for the refractive-index variation (Δn) calculation based on the measured value of the fringe shift can be derived from the geometric considerations of differences of optical path lengths shown in Fig. 1. The actual geometry of the experiment allowed us to use the following approximate expression for Δn:

$$\Delta n = \frac{\lambda \Delta S}{2t}, \tag{4}$$

where λ is the wavelength of the probe beam (633 nm), ΔS is the fractional fringe shift, and t is the thickness of the sample. The accuracy of formula (4) compared with the exact solution is better than 0.5%, and consequently it can be used for data processing. Thus the refractive-index variation of the glass sample can be calculated along the direction of the interference fringe. The interference pattern was detected with the CCD camera as a picture with 640 × 480 pixels. For the standard experimental arrangement, the spatial resolution in the y direction (Fig. 3) was ~10 μm, while in the x direction it was ~250 μm because of the shift of the interfering beams. An accuracy of the phase-shift determination in this case was limited by the distance between pixels in the CCD camera and the noise. To increase it, the Fourier transform of this signal over the whole row in the x direction was performed, the fundamental sinusoidal function was selected, and, finally, the phase shift of the fundamental harmonic for each row was found. The increment of this phase with respect to the first row was calculated, and the refractive-index change in each row was found with Eq. (4). This procedure degrades the spatial resolution in the x direction up to a few millimeters but improves the sensitivity of the measurement by orders of magnitude.

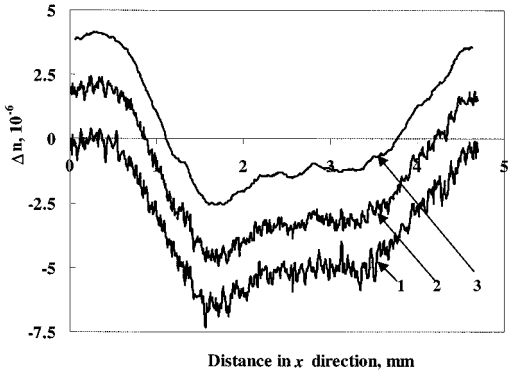

Fig. 4. Spatial profiles of the refractive index in the virgin sample of PTR glass: 1, single recording of the interference pattern at CCD camera; 2, combined result of two recordings; 3, averaging by 11 neighboring pixels at the CCD. Curves 2 and 3 are shifted up for 2×10^{-6} and 4×10^{-6}, respectively.

A number of virgin PTR glass samples were tested in this setup for evaluation of repeatability and sensitivity of the method. Spatial profiles of the refractive index calculated for the virgin sample in accordance with formula (4) are shown in Fig. 4. One can distinguish high-frequency and low-frequency spatial fluctuations in the profile (curve 1). High-frequency fluctuations are at the level of the ±0.002 fringe shift and correspond to the refractive-index fluctuations of $\pm 5 \times 10^{-7}$. It was found that these fluctuations could be decreased several times by multiple detection of the interference pattern and averaging of the phase shifts (or refractive indices). No stable high-frequency patterns were found after this procedure. An example of the data obtained from two measurements and further averaged is shown in Fig. 4, curve 2. It is important to note that the high-spatial-frequency fluctuations were mitigated while the low-spatial-frequency fluctuations were not affected by multiple measurements and averaging. This means that the high-frequency fluctuations can be considered as detection noise. As a result, fur-

ther averaging over 11 neighboring pixels at the CCD camera was performed (Fig. 4, curve 3). Finally, the sensitivity of the phase-shift measurement in the liquid-cell shearing interferometer was determined to be approximately $\pm 4 \times 10^{-4}$ of the fringe period. This value corresponds to a sensitivity in the measurement of the refractive-index fluctuations in a 1-mm-thick glass sample of $\pm 10^{-7}$.

Multiple measurements of the same area and for the same virgin sample have shown a repeatability of the spatial profile of the refractive index (Fig. 4). This means that those low-frequency fluctuations in Fig. 4 are real spatial fluctuations of the refractive index of tested samples, and actual refractive-index fluctuations in the selected laboratory-made virgin PTR glass samples ranged from 5×10^{-6} to 7×10^{-6} with a spatial scale of ~5 mm.

A number of conclusions can be made based on the interferometric mapping of the refractive index. First, the liquid-cell shearing interferometer is a precise tool for optical homogeneity measurements (spatial fluctuations of a refractive index) with a sensitivity of $\sim 10^{-7}$ and a spatial resolution in the x direction of approximately a few millimeters. Second, subtraction of the refractive-index spatial profiles of the same sample after consecutive stages of exposure and development provides an accuracy of the resulting refractive-index profile of approximately $\pm 2 \times 10^{-7}$. Third, the optical homogeneity of selected samples of fluorinated silicate glass (PTR glass) melted in a 400-ml silica crucible[5] is better than 10^{-5} at the scale of several millimeters, and therefore this glass can be used in most laser applications with little detectable contribution to the net distortion of the optical system.

B. Measurement of the Induced Index of Refraction

To provide both the high sensitivity of the induced refractive-index measurement and high spatial resolution, the following experimental arrangement was used. The specimen was placed into the liquid cell in such way that the lateral shift of the probe beam in the interferometer was directed along the irradiated stripe (see Subsection 2.C). The rows of the CCD camera used for pattern detection were aligned along the same direction (x). An example of the interference pattern detected in the 1-mm sample irradiated with the maximum dosage of ~0.6 J/cm^2 is shown in Fig. 5. One can see a uniform interference pattern with a rather low level of noise. The lack of bipolar fringe deviations indicates the absence of peculiarities on the borders of the exposed area. Optical distortions (phase shifts) occupy the region of illumination, and no noticeable spreading of the phase shifts outside of this area was detected. The direction of the fringe shift corresponded to a decrease of the refractive index in the exposed area.

Thus the refractive-index decrement for each horizontal line (x) in the interference pattern in Fig. 5, which is a line of equal dosage, can be calculated with formula (4). One can see in Fig. 5 that the periodic interference pattern is slightly distorted by some

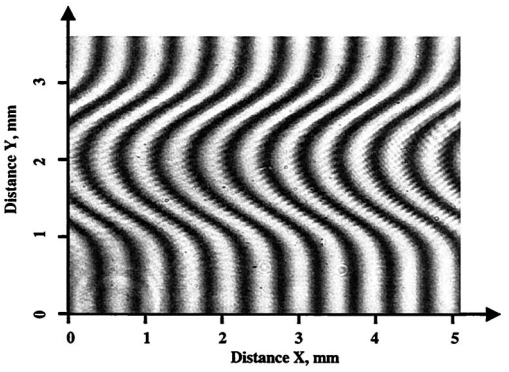

Fig. 5. Interference pattern from PTR glass (1-mm thickness) exposed to the straight stripe with a lateral Gaussian profile (half-width $1/e^2M$ = 1.24 mm) of the He–Cd laser at 325 nm for the maximum dosage of 600 mJ/cm^2 in the center of the stripe and thermally developed for 2 h at 520 °C. The laser beam was scanned across the sample in the horizontal direction.

noise produced by parasitic diffraction and interference caused by defects and optical system imperfections. To increase the accuracy of the phase-shift determination, the same procedure of averaging with Fourier transform was used as that in Subsection 3.A.

The next step was to assign to each horizontal line in Fig. 5 the value of the exposing dosage. The procedure of intensity distribution measurement was described in Subsection 2.C. The best-fit Gaussian function describing the experimental intensity distribution is shown in Fig. 6, curve 1. The image of the interference pattern from the CCD camera was preliminarily calibrated, and the spatial scale of the image was obtained. Knowing the spatial scale of the interference pattern image allowed us to calculate the spatial distribution of the refractive-index decrement, which is shown in Fig. 6, curve 2. One can see that this experimental curve has a smooth shape with no modulation, peaks, or dips. The absence of these features indicates that the spectral filtering in the procedure of phase determination was effective enough to eliminate the effect of spatial noise seen in

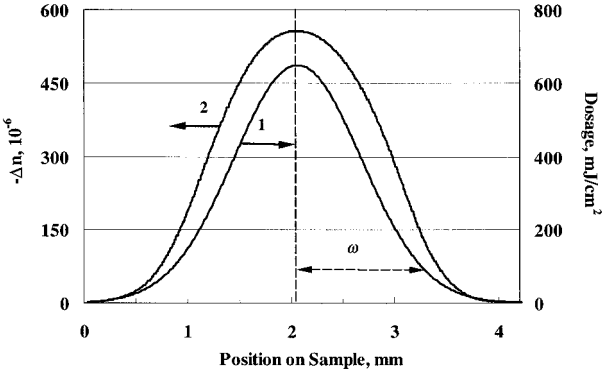

Fig. 6. Profiles of the dosage of laser radiation at 1, 325 nm and induced refractive index at 2, 633 nm in the exposed sample of PTR glass.

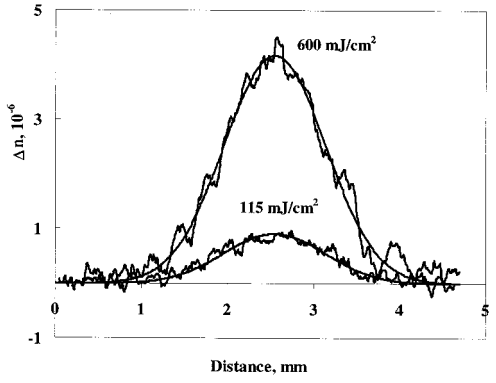

Fig. 7. Induced refractive-index profile in PTR glass exposed to radiation at 325 nm with maximum exposures of 115 and 600 mJ/cm^2 (no thermal development).

the interference pattern (Fig. 5). An important point is that the superposition of the maxima of the exciting-beam intensity spatial distribution (Fig. 6, curve 1) and the refractive-index increment (Fig. 6, curve 2) provides an opportunity to find a direct correspondence between dosage and the refractive-index decrement, which will be discussed below. This means that the procedure described above provides a functional dependence of the induced refractive index versus exposing dose by analysis of a single exposed pattern at a sample of the photosensitive material.

C. Refractive-Index Increment after UV Exposure

It is known that the ionizing action of radiation on silicate glasses causes not only induced absorption but also refractive-index changes and birefringence, which were described in Refs. 10–13. This induced refraction was detected at the level of $\sim 10^{-6}$, and its origin was derived from both polarizability variations and stresses caused by photoinduced structural transformations. It was found that the short-UV radiation having $\lambda < 250$ nm and x rays or γ rays can cause these effects. The spectral region of photosensitivity of PTR glass[4] is in the near UV, and it is usually assigned to the absorption band of Ce^{3+}, having a maximum at 305 nm. It is clear that no silicate glass matrix ionization can occur and no intrinsic hole centers can be generated in silicate glass under exposure to near-UV radiation (Ref. 14, p. 8). Only transformations of the valence forms of the different dopants and the electron color center generation that results in additional absorption have been observed in the PTR glass after such excitation.[4] However, no data on refractive-index changes after exposure to UV radiation have been published for the PTR glass. Therefore it was not clear if a photoinduced refraction could be observed in the PTR glass under exposure to radiation at 325 nm if no heat treatment was applied to the exposed sample.

To study induced refraction in PTR glasses after UV irradiation, a refractive-index profile of the same area was measured before and after UV exposure. The differences in the refraction profiles recorded after and before UV exposure are shown in Fig. 7 for two different dosages. The smooth curves are the Gaussian functions with the width (ω = 1.24 mm) equal to that of the exciting UV beam. One can see that the spatial profile of the induced index of refraction coincides with the spatial profile of the exposing radiation and that the value of the induced refractive index is approximately proportional to dosage. It is important to note that UV exposure of PTR glass (with no thermal treatment) results in an increment (not decrement) in the refractive index similar to that of undoped silicate glasses[10–13] but opposite to that for radiation-hardened glasses doped with a high concentration of cerium.[12,13] The role of cerium in photoinduced refraction should be the subject of separate research. It was found that heat treatment of an exposed PTR glass up to 480 °C decreased the value of the induced refractive index whereas heating above 500 °C changed the sign of the effect and a decrement of the refractive index was observed (see Subsection 3.D). This decrease could be caused by thermal bleaching of different intrinsic color centers of the glass matrix, as was described in Refs. 10 and 11 for undoped optical glasses. However, in PTR glass containing silver and fluorine,[4] no thermal bleaching of additional absorption was observed, although two additional processes occur at the elevated temperature. They are precipitation of colloidal silver particles at a temperature of ~450 °C and precipitation of the NaF crystalline phase at temperatures above 500 °C.[4] The absence of any peculiarities of induced refractive index in the range of 450 °C allows us to conclude that colloidal silver precipitation did not cause a detectible negative PTR effect. The last effect is triggered by NaF crystalline-phase precipitation at higher temperatures. This means that both color center bleaching and initial stages of the negative PTR effect can contribute to the decrease of the induced refractive index under the heat treatment below 480 °C.

D. Refractive-Index Decrement after UV Exposure Followed by Thermal Development

The basic properties of any photosensitive media are photosensitivity (for phase recording, this is the derivative of the refractive-index increment over the exposing dose) and reciprocity (independence of the refractive-index increment on irradiance for the same dose; see, e.g., Ref. 15). The reciprocity law for induced absorption was demonstrated in silicate glasses exposed to short-wavelength UV radiation that generated intrinsic color centers.[16] However, photochromic glasses doped with halide nanocrystals did not show reciprocity because of partial bleaching in the process of irradiation (Ref. 14, p. 96). The refractive-index decrement in PTR glasses as a result of UV exposure followed by thermal development was described in early publications,[4] but no direct measurements of induced refraction dependence on dosage and the irradiance of exciting radiation were performed for those publications.

To observe these characteristics of PTR glasses, we exposed the sample to the scanned Gaussian beam at

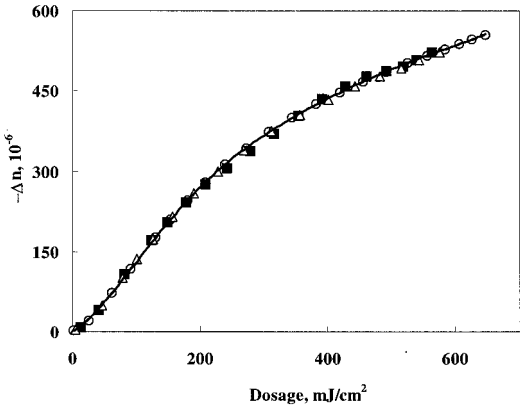

Fig. 8. Dependence of the refractive-index decrement on the dosage of exciting radiation at 325 nm for different values of maximum irradiance. Circles, 20 mW/cm^2; triangles, 4 mW/cm^2; squares, 1 mW/cm^2. The thermal development was 2 h at 520 °C.

325 nm, as described in Subsection 2.C. Three Gaussian stripes were irradiated in the 1-mm-thick glass specimen with the same maximum dosage of 600 mJ/cm^2. The difference between the stripes was in the total power of the exciting beam and consequently in different maximum irradiances for each stripe. Maximum irradiance for the first stripe was $\sim$20 mW/cm^2. The beam powers for the second and the third stripes were attenuated by 5× and 20× glass-absorbing filters, respectively. The velocity of the beam scanning in these cases was decreased proportionally. The total beam power and lateral beam profile were measured before and after irradiation to be sure that no laser power fluctuations, UV filter transmission deterioration (see, e.g., Ref. 17), or induced lensing occurred in the process of exposing the samples. The sample was subjected to the standard development procedure from 1 to 8 h at 520 °C.[5]

The dependence of the induced refractive index on the exposing dose after 2 h of thermal development for all three stripes is shown in Fig. 8. One can see that there is no difference in the refractive-index decrement for the different values of irradiance. An independence of induced refraction on irradiance was observed for all periods of thermal development. This means that PTR glass obeys the reciprocity law and the induced index of refraction depends on total dosage only. Another consequence of this result is the ability to reconstruct the whole dependence of refractive-index decrement on dosage by mathematical treatment (Subsection 3.A) of the single irradiated stripe (Fig. 8). An induced refractive index exhibited a curve with a continuously decreasing slope. The maximum value of the refractive-index increment was $\sim 10^{-3}$. One can see that the refractive-index decrement depends linearly on dosage up to 3×10^{-4}. Inside this region an approximate value of the photosensitivity ($\Delta n/D$) of PTR glass for 325-nm irradiation followed by 3 h of development at 520 °C is 1.5×10^{-3} cm^2/J. It is important to note that the coincidence of the induced index of refraction in all exposed stripes shows that the photosensitivity of used PTR glass is constant all over the specimen.

4. Conclusions

The following points summarize our findings:

- A liquid-cell shearing interferometer is developed that enables a measurement of the volume refractive-index distribution in solid specimens with an accuracy of $\sim 10^{-7}$ with spatial resolution in the x direction of approximately a few millimeters and is not sensitive to surface imperfections of the sample. An interferometer can be used for both optical homogeneity and induced refraction measurements. The dynamic range of measurement was $\sim$4 orders of magnitude.
- A method is developed for measurement of the dependence of the induced index of refraction on dosage of exciting radiation in photosensitive materials by treatment of a single irradiated pattern, which is a straight stripe with a Gaussian lateral profile of irradiance.
- Exposure of PTR glass to near-UV radiation at 325 nm results in refractive-index increment ranging up to 5×10^{-6}.
- Exposure of PTR glass to near-UV radiation followed by thermal development results in a refractive-index decrement ranged up to 10^{-3}. Its photosensitivity for phase recording is approximately 1.5×10^{-3} cm^2/J.
- PTR glass obeys the reciprocity law, i.e., the induced refraction depends on exposing dose and does not depend on the irradiance of the exciting radiation.

This research has been supported by Ballistic Missiles Defense Organization (BMDO) contracts 66001-97-C60008 and 66001-00-C-7005. The authors are grateful to L. N. Glebova for the glass melting and preparing the samples and to C. M. Stickley for the fruitful comments and discussion.

References

1. P. Hariharan, "Practical recording materials," in *Optical Holography: Principles, Techniques, and Applications* (Cambridge University, New York, 1996), Chap. 7, pp. 95–97.
2. K. O. Hill, Y. Fujii, D. C. Jhonson, and B. S. Kawasaki, "Photosensitivity in optical fiber waveguides: Application to reflection filter fabrication," Appl. Phys. Lett. **32,** 647–649 (1978).
3. G. Meltz, W. W. Morey, and W. H. Glenn, "Formation of Bragg gratings in optical fibers by transverse holographic method," Opt. Lett. **14,** 823–825 (1989).
4. L. B. Glebov, "Photosensitive glass for phase hologram recording," Glastech. Ber. **71C,** 85–90 (1998).
5. O. M. Efimov, L. B. Glebov, L. N. Glebova, K. C. Richardson, and V. I. Smirnov, "High-efficiency Bragg gratings in photothermorefractive glass," Appl. Opt. **38,** 619–627 (1999).
6. O. M. Efimov, L. B. Glebov, and V. I. Smirnov, "High-frequency Bragg gratings in photothermorefractive glass," Opt. Lett. **23,** 1693–1695 (2000).
7. M. Born and E. Wolf, *Principles of Optics* (Cambridge University, Cambridge, UK, 1999), pp. 348–352.

8. M. V. R. K. Murty, "The use of a single plane parallel plate as a lateral shearing interferometer with a visible gas laser source," Appl. Opt. **3,** 531–534 (1964).
9. D. W. Griffin, "Phase-shifting shearing interferometer," Opt. Lett. **26,** 140–141 (2001).
10. L. B. Glebov, V. G. Dokuchaev, N. V. Nikonorov, and G. T. Petrovskii, "New effect of the interaction of optical radiation with glass," Sov. Phys. Dokl. **29,** 57–58 (1984).
11. L. B. Glebov, V. G. Dokuchaev, and N. V. Nikonorov, "Glass matrix strain caused by photoinduced charging of point defects," J. Non-Cryst. Solids **128,** 166–171 (1991).
12. A. O. Volchek, A. I. Gusarov, A. L. Diikov, and F. N. Ignat'ev, "Change of the refractive index of silicate glasses under ionizing radiation," Glass Phys. Chem. **21,** 107–110 (1995).
13. A. I. Gusarov and D. B. Doyle, "Radiation-induced wave-front aberrations: a new approach," Appl. Opt. **37,** 643–648 (1998).
14. A. V. Dotsenko, L. B. Glebov, and V. A. Tsekhomsky, *Physics and Chemistry of Photochromic Glasses* (CRC Press, Boca Raton, Fla., 1997).
15. N. Mott and R. W. Gurney, *Electronic Processes in Crystals* (Oxford University, Oxford, UK, 1948), Chap. 7.
16. L. B. Glebov and M. N. Tolstoi, "Spectra of formation of color centers in laser glasses," Sov. J. Quantum Electron. **4,** 65–67 (1974).
17. A. P. Gagarin, L. B. Glebov, O. M. Efimov, and O. S. Efimova, "Formation of color centers in sodium calcium silicate glasses with the nonlinear absorption of powerful UV radiation," Sov. J. Glass Phys. Chem. **5,** 337–340 (1979).